

Orbital-selective magnetism in FeAs-based superconductors

Hyungju Oh, Donghan Shin, and Hyoung Joon Choi*
 Department of Physics and IPAP, Yonsei University, Seoul 120-749, Korea
 (Dated: December 13, 2010)

We report first-principles studies of lanthanide-series (Ln) iron oxypnictides LnFeAsO (Ln=La, Ce, Pr, Nd, Sm, and Gd) which show two competing orbital-selective magnetic phases in small-Fe-moment regime: an in-plane d_{xy} magnetic phase, itinerantly driven by orbital selection of Fermi-surface nesting, and an out-of-plane d_{yz} magnetic phase, driven by local interactions. The Fe magnetic moments in the two phases show different coupling strengths to Fermi-surface electrons orbital-selectively, suggesting different roles in superconductivity and in antiferromagnetism, and making orbital characters of the moment resolvable by measuring the electronic structures. These results show that orbital sensitivity is a key factor in the magnetic properties of FeAs-based materials.

PACS numbers: 71.15.Mb, 71.20.-b, 74.70.Xa, 75.25.-j

$\text{LaFeAsO}_{1-x}\text{F}_x$ [1] and related compounds show unconventional superconductivity (SC) in the vicinity of antiferromagnetism (AFM) [2–16]. Among various families of iron pnictides and chalcogenides, lanthanide-series (Ln) iron oxypnictides LnFeAsO reach the highest superconducting transition temperature (T_c) with doping. Reported T_c in doped LnFeAsO increases dramatically from 26 K up to 55 K with Nd or Sm substitution for La and then T_c decreases slightly in doped GdFeAsO [1, 2, 8, 11–15]. With this strong variation of T_c , LnFeAsO is suited for studying material dependence of T_c . Since FeAs-based materials are featured with multiple Fermi surfaces (FSs) with strong orbital characters, many studies have been done on FS nesting, local-moment interactions, and orbital orderings [17–27]. However, no specific feature has been pinpointed in electronic and magnetic properties correlated with material dependence of T_c except for As positions and their effect on FS.

In this Letter, we report, for the first time, orbital-selective magnetic phases in FeAs-based materials found by first-principles density functional theory (DFT) calculations. Two phases are identified with distinctive orbital characters of Fe magnetic moments, d_{xy} and d_{yz} , which originate from FS nesting and local interactions, respectively. The two phases, while competing with each other, show different electronic band structures caused by orbital-selective coupling strengths between Fe magnetic moments and FS electrons. Our results suggest that spin or magnetic interactions for unconventional SC should have strong orbital sensitivity in FeAs-based materials.

Our calculations are based on *ab initio* norm-conserving pseudopotentials and the Perdew-Burke-Ernzerhof-type generalized gradient approximation, as implemented in the SIESTA code [28]. During self-consistent iterations, constraints are imposed on the electron spin density to reduce the size of the Fe magnetic moment (m_{Fe}) to specific values smaller than unconstrained results. We assume an oxidation state of +3 for all considered Ln elements, treating their 4f orbitals as core orbitals [29, 30]. Experimental lattice constants

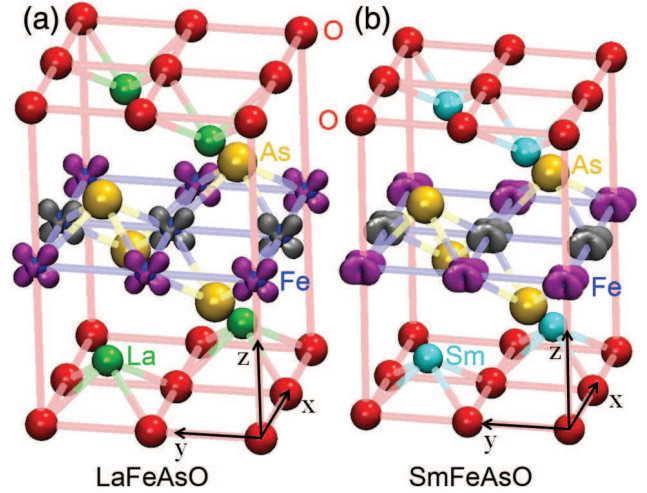


FIG. 1: (Color online). Orbital characters of Fe magnetic moments: (a) LaFeAsO and (b) SmFeAsO when m_{Fe} is 0.15 μ_B per Fe atom. Each atomic structure is a $\sqrt{2} \times \sqrt{2} \times 1$ supercell with four Fe atoms in the single-stripe-type AFM. Fe magnetic moments, in dark and light gray (purple and light gray), are ordered antiferromagnetically along the x axis and ferromagnetically along the y axis. Calculated Fe magnetic moments have two distinct orbital shapes, d_{yz} in LaFeAsO and d_{xy} in SmFeAsO . The considered m_{Fe} of 0.15 μ_B is about one half of experimental values, 0.36 μ_B in LaFeAsO [3] and 0.34 μ_B in SmFeAsO [14].

and atomic positions at the high-temperature tetragonal phase are used for the calculations [3, 4, 9, 10, 15, 31].

An intriguing new finding in our present work is Ln-dependent distinctive d -orbital characters of the Fe magnetic moment in LnFeAsO in small m_{Fe} regime. Figure 1 shows two prototypical cases of LaFeAsO and SmFeAsO . For m_{Fe} of 0.15 Bohr magneton (μ_B) per Fe atom, LaFeAsO shows out-of-plane d_{yz} character, but SmFeAsO shows in-plane d_{xy} character. In previous studies, the main concern was not d_{xy} versus d_{yz} , but d_{yz} versus d_{zx} regarding symmetry lowering from tetragonal to orthorhombic structures. In our work, symmetry

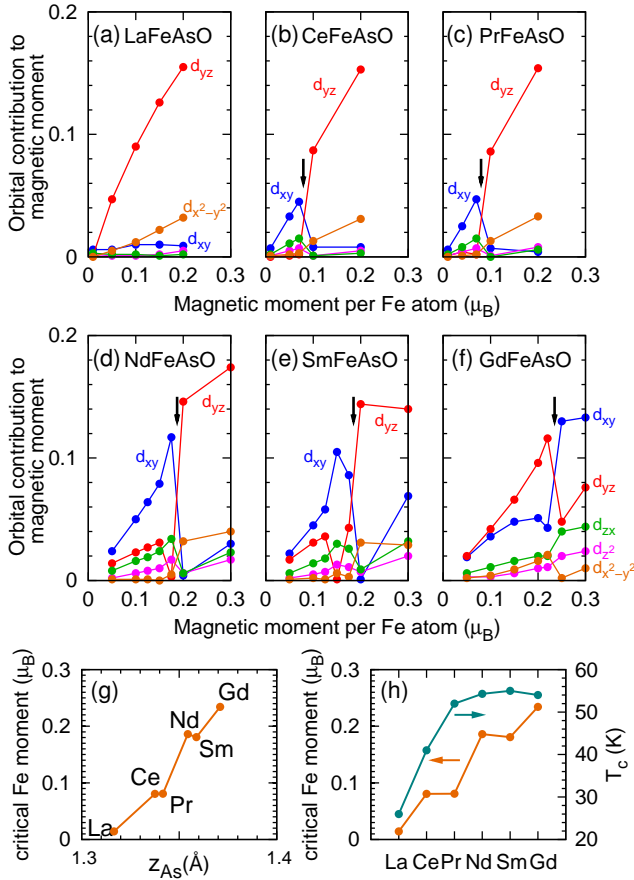


FIG. 2: (Color online). Orbital analysis of Fe magnetic moments in LnFeAsO. (a)-(f) Orbital contribution to the Fe magnetic moment as a function of m_{Fe} per Fe atom in LnFeAsO. Downward arrows indicate critical values of m_{Fe} at which orbital characters switch between d_{xy} and d_{yz} . In LaFeAsO, the critical m_{Fe} is very close to zero. (g) Critical m_{Fe} versus the As height from the Fe layer. (h) Ln-dependences of critical m_{Fe} and experimental T_c . Experimental T_c 's are 26 K in LaFeAsO_{0.89}F_{0.11} [1], 41 K in CeFeAsO_{0.84}F_{0.16} [8], 52 K in PrFeAsO_{0.89}F_{0.11} [11], 54.3 K in NdFeAsO_{1-y} [13], 55 K in SmFeAsO_{0.9}F_{0.1} [12], and 54 K in GdFeAsO_{1-y} [13].

is lowered by imposing the single-stripe-type AFM, yet d_{xy} character is predominant in SmFeAsO.

For systematic study, we analyze orbital contributions to the Fe magnetic moment in LnFeAsO as a function of m_{Fe} [Figs. 2(a)-(f)]. We find that either d_{xy} or d_{yz} character is dominant, switching abruptly at a critical value of m_{Fe} in each compound. The critical m_{Fe} is 0.014 μ_B in LaFeAsO and increases to 0.23 μ_B in GdFeAsO. Except for GdFeAsO, the d_{xy} (d_{yz}) character appears at smaller (larger) m_{Fe} than the critical value. In LaFeAsO, the critical m_{Fe} is so small that the d_{yz} character is dominant [Fig. 2(a)]. In GdFeAsO, unlike other compounds, the d_{yz} character is larger than the d_{xy} character at m_{Fe} smaller than the critical moment [Fig. 2(f)].

The overall increase of the critical m_{Fe} from LaFeAsO

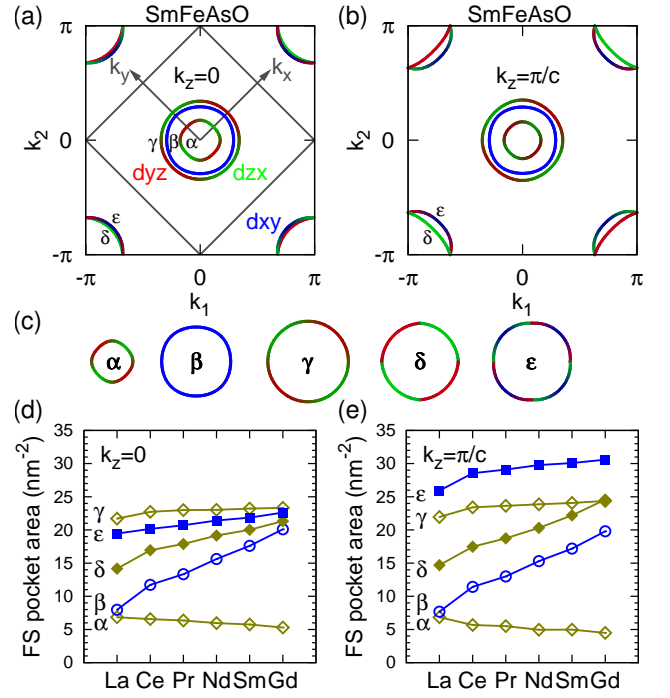


FIG. 3: (Color online). Orbital characters and pocket areas of Fermi surfaces (FSs) in nonmagnetic LnFeAsO. (a) FS of nonmagnetic SmFeAsO at $k_z = 0$ and (b) at $k_z = \pi/c$. The k_1 and k_2 axes are along reciprocal lattice vectors of the nonmagnetic unit cell having two Fe atoms. In (a), the 45°-rotated inner square is the first Brillouin zone of the $\sqrt{2} \times \sqrt{2} \times 1$ supercell having four Fe atoms, where k_x and k_y axes are along the x and y axes in Fig. 1(a), respectively. Three hole pockets (α , β , and γ) are located at the center and two electron pockets (δ and ϵ) at the corner. Orbital characters, d_{xy} , d_{yz} , and d_{zx} , are represented in blue, red, and green, respectively. The α , γ , and δ pockets are derived from d_{yz} and d_{zx} , the β pocket is from d_{xy} , and the ϵ pocket is from d_{xy} , d_{yz} , and d_{zx} . (c) FS pockets at $k_z = 0$. The δ and ϵ pockets are plotted as closed loops to highlight changes in orbital characters around the pockets. (d) Areas of the five FS pockets at $k_z = 0$ and (e) at $k_z = \pi/c$ as a function of Ln elements.

to GdFeAsO is correlated most strongly with the increase of the As height from the Fe plane among various structural parameters [Fig. 2(g)], and correlated with experimentally reported T_c [Fig. 2(h)]. This suggests that the d_{xy} magnetic moment is closely related with measured T_c in the doped LnFeAsO for Ln from La to Sm, while GdFeAsO shows different and more complicated orbital features possibly because GdFeAsO is beyond an optimal chemical composition for T_c [1, 2, 8, 11–15].

To understand the origin of the orbital-distinctive magnetic moments, we analyzed orbital characters of FS in nonmagnetic LnFeAsO. As a prototype, SmFeAsO has three cylindrical hole pockets [α , β , and γ in Figs. 3(a)-(c)] and two electron pockets [δ and ϵ in Figs. 3(a)-(c)] at the Fermi energy (E_F). Orbital analysis shows that the α , γ , and δ pockets are derived from Fe d_{yz} and d_{zx}

orbitals, the β pocket is from d_{xy} , and the ϵ pocket is from d_{xy} , d_{yz} , and d_{zx} [Figs. 3(a)-(c)]. For FS nesting, we consider six pairs of hole and electron pockets: α - δ , β - δ , γ - δ , α - ϵ , β - ϵ , and γ - ϵ . Among these, α - δ nesting is not significant because the two pockets have quite different pocket areas in all LnFeAsO [Figs. 3(d) and (e)], and β - δ nesting is not effective because orbital difference of the two pockets degrades effects of nesting greatly. In addition, γ - δ and α - ϵ nesting effects should be very weak because of orbital mismatch due to out-of-phase alternations of d_{yz} and d_{zx} characters around the pockets. Thus, we need to examine only β - ϵ and γ - ϵ nesting regarding the orbital character of the Fe magnetic moment.

Since the β -hole pocket is derived from the d_{xy} orbital, β - ϵ nesting may induce Fe magnetic moment of d_{xy} character. Similarly, γ - ϵ nesting may induce Fe magnetic moment of d_{yz} or d_{zx} character. Calculated FS pocket areas as a function of Ln elements [Figs. 3(d) and (e)] show that the β -hole pocket area is sensitive to Ln elements, approaching the ϵ -electron pocket area for heavier Ln elements, while the γ -hole pocket area is almost insensitive to Ln elements and close to the ϵ -electron pocket area. This indicates that β - ϵ FS nesting is a key factor in the electronic structures in LnFeAsO which changes the orbital character of the Fe magnetic moment.

Although it is not involved in the FS nesting, the area of the δ -electron (d_{yz} and d_{zx}) pocket also depends sensitively on Ln elements [Figs. 3(d) and (e)]. With heavier Ln elements, the β -hole (d_{xy}) band moves upward in energy and the δ -electron band moves downward in energy, resulting in electron transfer from the d_{xy} orbital to the d_{yz} and d_{zx} orbitals. Since the δ -pocket is not related with FS nesting, the increased d_{yz} and d_{zx} electrons can contribute to magnetic moments only by non-FS-nesting mechanism, e.g., local-moment interactions [7, 16]. Therefore, while the enhanced d_{xy} magnetic moment from LaFeAsO to SmFeAsO is due to better β - ϵ FS nesting, the enhanced d_{yz} magnetic moment in GdFeAsO is due to increased d_{yz} electrons in the δ -pocket which favor non-FS-nesting mechanism.

To find out effects of different orbital characters of Fe magnetic moments on the electronic structures, we obtained orbital-resolved band structures and projected density of states (PDOS) in SmFeAsO, as a prototype of LnFeAsO, in nonmagnetic and magnetic phases (Fig. 4). With zero m_{Fe} , energy bands have distinct orbital characters along high-symmetry lines, yielding PDOS slowly varying near E_F [Figs. 4(a) and (b)].

With the d_{xy} magnetic moment, strong anti-crossing occurs between d_{xy} bands, opening orbital-dependent energy gaps at E_F [Fig. 4(c)]. In the ΓX line, d_{xy} and d_{zx} bands repel each other at E_F and at -260 meV. In the ΓY line, d_{xy} bands open a large energy gap near E_F [marked with Δ_{xy} in Fig. 4(c)], while d_{zx} bands are intact. Except for anti-crossing at -100 meV in the ΓY line, d_{yz} bands are almost unchanged. The d_{xy} PDOS is greatly modified

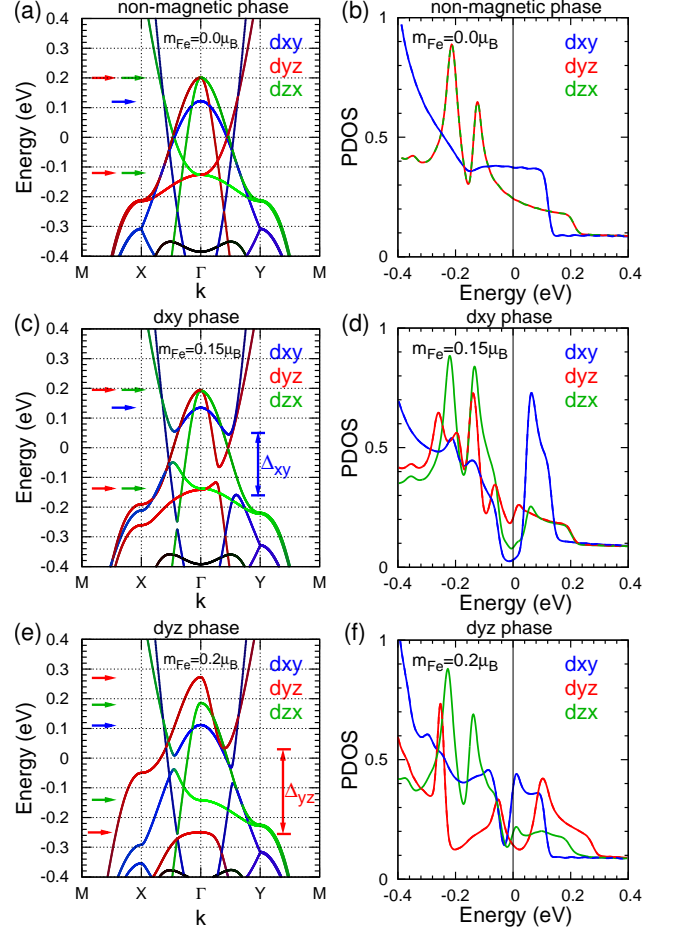


FIG. 4: (Color online). Orbital-resolved electronic band structures and projected density of state (PDOS) in SmFeAsO: (a) and (b) for nonmagnetic phase, (c) and (d) for the d_{xy} phase ($m_{Fe} = 0.15 \mu_B$), and (e) and (f) for the d_{yz} phase ($m_{Fe} = 0.20 \mu_B$). Band structures are plotted along high-symmetry lines in the first Brillouin zone of the $\sqrt{2} \times \sqrt{2} \times 1$ supercell for the single-stripe-type AFM, where M = (0, π), X = ($\pi/2$, $\pi/2$), Γ = (0, 0), and Y = ($-\pi/2$, $\pi/2$) with respect to the unit-cell reciprocal axes, k_1 and k_2 , shown in Fig. 3(a). Blue, red, and green represent d_{xy} , d_{yz} , and d_{zx} orbital characters, respectively, and E_F is set to zero. Horizontal arrows indicate extreme band energies at Γ . In (c), Δ_{xy} indicates energy gap between d_{xy} bands in the ΓY line. In (e), Δ_{yz} indicates energy gap between d_{yz} bands in the ΓY line.

fied with a partial-gap opening at E_F and a huge peak right above E_F [Fig. 4(d)]. The d_{zx} PDOS also shows a reduction near E_F because of coupling to d_{xy} [Fig. 4(d)]. Despite these large effects of the d_{xy} magnetic moment on the electronic structures near E_F , deformation of bands is mostly near the crossing points, with no shift of original band edges [Fig. 4(c)]. This confirms that the origin of the d_{xy} magnetic moment is due to FS nesting.

In contrast, with the d_{yz} magnetic moment, d_{yz} bands are deformed in the whole Brillouin zone much more greatly than anti-crossing of bands [Fig. 4(e)]. Whole

upper part of d_{yz} bands and whole lower part of d_{yz} bands are expelled from each other [Fig. 4(e)], so even the top of the d_{yz} hole band is pushed up by 100 meV and the bottom of the d_{yz} electron band is pushed down by 100 meV. This change of d_{yz} bands in the whole Brillouin zone indicates that the driving mechanism for the d_{yz} magnetic moment is not FS nesting (local in k-space) but lowering of the total energy of electrons by formation of local magnetic moments (local in real space). Despite the large change in the d_{yz} bands, all the other bands are almost unchanged except for some anti-crossings.

Since different orbital characters of the Fe magnetic moment result in orbital-dependent difference in electronic structures, the orbital characters of the Fe magnetic moment can be distinguished by, e.g., angle-resolved photoemission spectroscopy of detwinned samples [27, 32]. As established by previous studies, DFT electronic band structures are qualitatively consistent with experimental results in FeAs-based materials although the DFT results overestimate experimental bandwidths by a factor of 2 to 3 near E_F . Thus, detailed comparison of our band structures with experimental results will reveal orbital characters of the Fe magnetic moment, and thereby their roles in AFM.

As shown above, the d_{xy} magnetic moment is driven by orbital-selective FS nesting, while the d_{yz} magnetic moment is related with spatially localized interactions such as local-moment interactions. Thus, the competition of d_{xy} and d_{yz} magnetic moments in LnFeAsO is itinerant versus local-moment magnetisms. In addition, when m_{Fe} is increased to $1.0 \mu_B$ and higher, the Fe magnetic moment evolves gradually to an almost spherical shape with no specific orbital characters. Thus, the orbital-distinctive magnetic moments and their effects will appear with different strengths in various iron pnictides and chalcogenides for the wide range of reported m_{Fe} .

In conventional SC, electron-phonon interactions depend on phonon polarizations, and too large interactions may induce structural changes that suppress SC. Likewise, the Fe magnetic moment in LnFeAsO may have different roles in SC and AFM depending on its orbital character. Since our results show that the d_{yz} character couples more strongly to electrons than the d_{xy} one, a possibility is that the former drives AFM while the latter mediates SC. Another possibility is that only the d_{xy} character is significant in both AFM and SC, which could be relevant if the d_{yz} character has much weaker coupling to electrons in real samples than our results due to, e.g., fluctuations. An opposite scenario is that only the d_{yz} character is significant in AFM and SC, which is less likely according to our result that SmFeAsO, having much higher T_c than LaFeAsO when doped, shows the strong d_{xy} character while LaFeAsO shows the d_{yz} one.

In conclusion, we have found that Fe magnetic moment in LnFeAsO (Ln = La to Gd) has distinctive orbital character, d_{xy} or d_{yz} , depending on Ln and m_{Fe} . With orbital

analysis of electronic structures, we have shown that the origins of the d_{xy} and d_{yz} orbital characters of the Fe magnetic moment are FS nesting and local interactions, respectively. These orbital characters have different coupling strength to FS electrons, so they can be identified by orbital-sensitive measurement of electronic structures and they may have different roles in SC and AFM. These results pave the way for understanding the role of spin or magnetic interactions in FeAs-based superconductors.

This work was supported by the NRF of Korea (Grant No. 2009-0081204). Computational resources have been provided by KISTI Supercomputing Center (Project No. KSC-2008-S02-0004).

* Email: h.j.choi@yonsei.ac.kr

- [1] Y. Kamihara *et al.*, J. Am. Chem. Soc. **130**, 3296 (2008).
- [2] X. H. Chen *et al.*, Nature (London) **453**, 761 (2008).
- [3] C. Cruz *et al.*, Nature (London) **453**, 899 (2008).
- [4] J. Zhao *et al.*, Nature Materials **7**, 953 (2008).
- [5] Z. Yin *et al.*, Phys. Rev. Lett. **101**, 047001 (2008).
- [6] I. I. Mazin, D. J. Singh, M. D. Johannes, and M. H. Du, Phys. Rev. Lett. **101**, 057003 (2008).
- [7] T. Yildirim, Phys. Rev. Lett. **101**, 057010 (2008).
- [8] G. F. Chen *et al.*, Phys. Rev. Lett. **100**, 247002 (2008).
- [9] Y. Qiu *et al.*, Phys. Rev. Lett. **101**, 257002 (2008).
- [10] J. Zhao *et al.*, Phys. Rev. B **78**, 132504 (2008).
- [11] Z. A. Ren *et al.*, Mater. Res. Innov. **12**, 105 (2008).
- [12] Z. Ren *et al.*, Chin. Phys. Lett. **25**, 2215 (2008).
- [13] K. Miyazawa *et al.*, J. Phys. Soc. Jpn. **78**, 034712 (2009).
- [14] Y. Kamihara *et al.*, New J. Phys. **12**, 033005 (2010).
- [15] P. Wang *et al.*, J. Phys. Condens. Matter **22**, 145701 (2010).
- [16] C. Y. Moon and H. J. Choi, Phys. Rev. Lett. **104**, 057003 (2010).
- [17] S. Lebegue, Phys. Rev. B **75**, 035110 (2007).
- [18] D. H. Lu *et al.*, Nature (London) **455**, 81 (2008).
- [19] D. J. Singh and M. H. Du, Phys. Rev. Lett. **100**, 237003 (2008).
- [20] K. Haule, J. H. Shim, and G. Kotliar, Phys. Rev. Lett. **100**, 226402 (2008).
- [21] C.-Y. Moon, S. Y. Park, and H. J. Choi, Phys. Rev. B **78**, 212507 (2008).
- [22] C.-C. Lee, W.-G. Yin, and W. Ku, Phys. Rev. Lett. **103**, 267001 (2009).
- [23] F. Krüger, S. Kumar, J. Zaanen, and J. van den Brink, Phys. Rev. B **79**, 054504 (2009).
- [24] C.-Y. Moon, S. Y. Park, and H. J. Choi, Phys. Rev. B **80**, 054522 (2009).
- [25] C. C. Chen *et al.*, Phys. Rev. B **82**, 100504(R) (2010).
- [26] W. Lv, F. Krüger, and P. Phillips, Phys. Rev. B **82**, 045125 (2010).
- [27] M. Yi *et al.*, arXiv:1011.0050.
- [28] D. Sánchez-Portal *et al.*, Int. J. Quantum Chem. **65**, 453 (1997).
- [29] I. A. Nekrasov, Z. V. Pchelkina, and M. V. Sadovskii, JETP Letters **87**, 560 (2008).
- [30] L. Pourovskii *et al.*, Europhys. Lett. **84**, 37006 (2008).
- [31] A. Martinelli *et al.*, J. Alloys Comp. **477**, L21 (2009).
- [32] Y. K. Kim *et al.*, arXiv:1011.1112.